THE JOURNAL OF BIOLOGICAL CHEMISTRY VOL. 283, NO. 37, pp. 25372–25380, September 12, 2008

T-box Protein Tbx18 Interacts with the Paired Box Protein Pax3 in the Development of the Paraxial Mesoderm*

Received for publication, April 8, 2008, and in revised form, June 27, 2008 Published, JBC Papers in Press, July 21, 2008, DOI 10.1074/jbc.M802723200

Henner F. Farin[‡], **Ahmed Mansouri**[§1], **Marianne Petry**[‡], **and Andreas Kispert**[‡2]

From the [‡]*Institute for Molecular Biology, Medizinische Hochschule Hannover, OE5250, Carl-Neuberg-Strasse 1, D-30625 Hannover, Germany and the* [§]*Department of Molecular Cell Biology, Max-Planck-Institute of Biophysical Chemistry, 37077 Göttingen, Germany*

The compartmentalization of somites along their anterior-posterior axis is crucial to the segmental organization of the vertebral column. Anterior-posterior somite polarity is generated in the anterior presomitic mesoderm by Mesp2 and Delta/Notch signaling and is further maintained by two transcriptional regulators, Uncx4.1 and Tbx18, acting in the posterior and anterior somite compartment, respectively. Here, we report that the paired box transcription factor Pax3 cooperates with the T-box protein Tbx18 in maintaining anterior somite half identity. Our findings that both genes are co-expressed in the anterior presomitic mesoderm and in early somites, that Pax3 and Tbx18 proteins physically interact, and that the loss of *Pax3* gene function enhances the vertebral defects (*i.e.* the gain of vertebral elements derived from posterior somite halves in *Tbx18* mutant mice) suggests that the two proteins cooperatively regulate the gene expression program necessary for maintaining anterior-posterior somite polarity. Genetic interaction of *Pax3* with *Tbx18* and the closely related T-box gene *Tbx15* was also observed in the development of the scapula blade, indicating an additional cooperative function for these genes in the paraxial mesoderm.

The metameric organization of the vertebral column derives from the somites, segmentally repeated units in the paraxial mesoderm. Somites form in a highly periodic and synchronized fashion by condensation and subsequent epithelialization of groups of mesenchymal cells at the anterior end of the presomitic mesoderm (PSM)[3] on both sides of the neural tube. Under the influence of signals from surrounding tissues, somites start to differentiate along their dorso-ventral axis. The ventral part undergoes an epithelial-mesenchymal transition to form the sclerotome, which contains precursors of the vertebral column and parts of the ribs. The dorsal part remains epithelial and generates the dermomyotome, from which skeletal muscles and the dermis of the skin will develop. In addition to differentiation along the dorso-ventral axis, somites become subdivided into distinct anterior and posterior compartments. Anterior-posterior (AP) polarization of somites underlies the segmental arrangement of the peripheral nervous system, since trajectories of neural crest and spinal nerves are confined to anterior somite halves. On the level of the sclerotome, the differential contribution of either compartment to the forming vertebra affects the structure of the axial skeleton. Vertebral bodies, laminae with the spinal processes, the rib heads, and the distal ribs derive from both somite halves, whereas pedicles with their transverse processes and proximal ribs derive from posterior somite halves only (1–3).

Establishment of somitic AP polarity is closely coupled to the segmentation process. Work from a variety of vertebrate model systems has shown that somite formation is governed by an oscillator known as the segmentation clock that operates in the PSM (4, 5). It is now believed that synchronized oscillations of a number of signaling pathways, including Wnt, fibroblast growth factor, and Notch signaling, are involved in the mechanism of the segmentation clock. Gradients of secreted signaling molecules cooperatively define the segmentation border within the anterior PSM. In this region, Notch oscillation is stabilized to a narrow domain, in which cells with a high Notch pathway activity will constitute the posterior half of a newly forming somite. In an adjacent stripe of cells, Notch signaling is suppressed by the action of the basic helix-loop-helix transcription factor Mesp2. The expression domain of *Mesp2* thereby defines the anterior somite half, and its anterior limit demarcates the next segmental border to be formed (6). Correspondingly, loss of Mesp2 activity leads to posteriorization of somites, whereas loss of *Delta-like1* (*Dll1*) gene function and Notch signaling results in somites that bear only features of anterior halves (7).

Molecular players required for the further maintenance of somitic AP polarity have recently surfaced. Genetic evidence from both loss- and gain-of-function studies in the mouse suggest that this process is controlled by the combined action of a pair of transcription factors, the T-box (Tbx) protein Tbx18 and the paired type homeobox protein Uncx4.1, which are expressed in anterior and posterior somite halves, respectively (8, 9). *Uncx4.1* is specifically required for the development of pedicles and proximal ribs (10, 11), elements exclusively derived from the posterior lateral sclerotome. In contrast, loss of *Tbx18* function results in expansion of pedicles and proximal ribs in the cervical and thoracic region of the axial skeleton (12). Notably, the forced misexpression of *Tbx18* in posterior somite

* This work was supported by grants from the German Research Council (Deutsche Forschungsgemeinschaft (DFG)) and by the DFG-funded cluster of excellence "REBIRTH" (to A. K.). The costs of publication of this article were defrayed in part by the payment of page charges. This article must therefore be hereby marked "*advertisement*" in accordance with 18 U.S.C. Section 1734 solely to indicate this fact.

[1] Supported by the Dr. Helmut Storz Stiftung and the Max-Planck-Society.

[2] To whom correspondence should be addressed. Tel.: 49-511-5324017; Fax: 49-511-5324283; E-mail: kispert.andreas@mh-hannover.de.

[3] The abbreviations used are: PSM, presomitic mesoderm; aa, amino acids; AP, anterior-posterior; E*n*, embryonic day *n*; NLS, nuclear localization sequence; GST, glutathione *S*-transferase; HA, hemagglutinin.

halves results in reduction of pedicles and proximal ribs (12), suggesting that Tbx18 is sufficient to specify anterior *versus* posterior somite fates. Opposing phenotypic consequences of loss of either factor are based on molecular cross-regulation. In *Uncx4.1* mutants, *Tbx18* expression is derepressed in posterior somite halves, whereas in *Tbx18* mutants, expression of *Uncx4.1* progressively expands in anterior somite halves (12). On the molecular level, Uncx4.1 may therefore act as transcriptional repressor of *Tbx18*, whereas Tbx18 may regulate *Uncx4.1* indirectly by controlling expression of the Notch ligand Dll1 (13). To get further insight into the molecular function of Tbx18, thus into the control of AP-somite compartmentalization, we sought to identify and characterize protein binding partners of Tbx18. This may also help to define transcriptional targets of Tbx18 and their molecular regulation.

Here, we report on the identification of the paired box (Pax) transcription factor Pax3 as a protein binding partner of Tbx18. We characterize this interaction on the biochemical level and define genetically that both transcription factors synergize in the development of the paraxial mesoderm, including anterior-posterior somite compartmentalization and scapula development.

EXPERIMENTAL PROCEDURES

Expression Constructs—Bacterial expression constructs were generated as N-terminal glutathione *S*-transferase (GST)-fusions in pGEX-4T3 (GE Healthcare). Generation of GST-Tbx18 fusion proteins has been described (13), and constructs covering the T-box region of mouse Tbx15 (aa 110–313), human TBX22 (aa 96–291), and mouse Brachyury (aa 41–225) were PCR-amplified from the cDNAs NM_009323, NM_016954, and NM_009309, respectively.

For *in vitro* expression of proteins, cDNA fragments were cloned with C-terminal Myc or HA tags in the vector pSP64 (Promega) that was modified to contain a 5′-β-globin leader and a 3′-β-globin trailer. Fragments encoding Pax3 partial (Fig. 1*D*) and full-length (aa 1–479) proteins were amplified from the mouse cDNA NM_008781. Expression plasmids of full-length Pax1 (aa 1–361), Pax7 (aa 1–503), and Pax9 (aa 1–342) were amplified from mouse cDNAs NM_008780, NM_011039, and NM_011041, respectively. For cytomegalovirus promoter/enhancer-driven expression in cells, the globin leader/cDNA/globin trailer cassette was shuttled into EcoRI and HindIII sites of pcDNA3 (Invitrogen). The expression vector for Tbx18ΔNLS has been described (13). All plasmids were sequenced; details on cloning strategies and primer sequences are available upon request.

Yeast Two-hybrid Screen—The construct for the generation of a fusion protein between the DNA binding domain of GAL4 and Tbx18 (aa 1–345) was cloned into pGBKT7 (Clontech). This bait vector was transformed into the yeast strain AH109 (Clontech), that was subsequently mated to the yeast strain Y187 that was pretransformed with a prey library of poly(T)-primed mouse embryonic day 11.5 (E11.5) whole embryo cDNAs (Clontech) following the manufacturer's instructions. Clones were selected on plates lacking leucine, tryptophan, histidine, and alanine. After this selection step, prey plasmids were isolated, amplified in *Escherichia coli*, and sequenced.

GST Pull-down, Immunofluorescence, and Co-immunoprecipitation Assays—These assays were performed as described (13).

Mice and Genotyping—Mice carrying a null allele of *Pax3* (*Pax3*^{lacZ}) (14), *Tbx18* (*Tbx18*^{tm2Akis} (12) (synonym: *Tbx18*^{GFP}), and *Tbx15* (*Tbx15*^{tm1Akis}) (15) (synonym: *Tbx15*^{lacZ}) were maintained on an outbred (NMRI) background. For the generation of compound mutants, double heterozygous mice were intercrossed. Genomic DNA prepared from yolk sacs or tail biopsies was used for genotyping by PCR (details on PCR strategies are available upon request). For timed pregnancies, vaginal plugs were checked in the morning after mating, and noon was taken as E0.5.

Skeletal Preparations—Skeletal preparations of E14.5 embryos and newborns were prepared essentially as previously described (12). Embryos were fixed in 95% ethanol overnight, and cartilaginous elements were then stained for 2 days in Alcian blue solution (150 mg/liter Alcian blue 8GX in 80% ethanol, 20% acetic acid). Embryos were transferred in methanol and cleared in benzylbenzoate/benzylalcohol (2:1).

In Situ Hybridization Analysis—Whole mount *in situ* hybridization analysis was performed with digoxigenin-labeled antisense riboprobes following a standard procedure (16). Stained specimens were transferred into 80% glycerol prior to documentation on a Leica M420 microscope with a Fujix digital camera HC-300Z. Images were processed in Adobe Photoshop CS. Details about probes are available upon request.

RESULTS

T-box and Pax Proteins Interact in Vitro—In order to identify protein interaction partners of Tbx18, we performed a yeast two-hybrid screen. We initially tested a number of fusion constructs of the GAL4-DNA-binding domain with subregions of Tbx18 protein for their quality as bait. A construct encoding a fusion protein with the N terminus and the T-domain of Tbx18, which was expressed and lacked autoactivation in yeast, was transformed into yeast, and the resulting bait strain was mated to a strain pretransformed with a mouse cDNA library from E11.5 whole embryos. One of the clones identified by the yeast two-hybrid screen harbored a partial cDNA for *Pax3*, a member of the gene family encoding paired box transcription factors (data not shown).

To validate and further investigate the interaction between Tbx18 and Pax3, we performed a series of *in vitro* binding assays using bacterially expressed subregions of Tbx18 fused to GST and *in vitro* expressed HA-tagged Pax3 protein (Fig. 1, *A* and *B*). In GST pull-down assays, Pax3 was specifically bound to GST-Tbx18 fusion proteins harboring the N-terminal domain and the T-box region (GST-Tbx18(N+T)) and the T-box region alone (GST-Tbx18(T)), respectively. Binding was observed neither with GST nor with GST-Tbx18(N) or GST-Tbx18(C), indicating that the T-domain of Tbx18 mediated the binding to Pax3 (Fig. 1*C*).

We next generated a series of deletion mutants of the *Pax3* cDNA for expression *in vitro* as HA-tagged peptides to determine which region of Pax3 confers interaction with Tbx18 (Fig. 1, *D* and *E*). Pax proteins are characterized by the presence of a conserved N-terminal DNA-binding region, the paired domain. Some of the eight murine family members, including

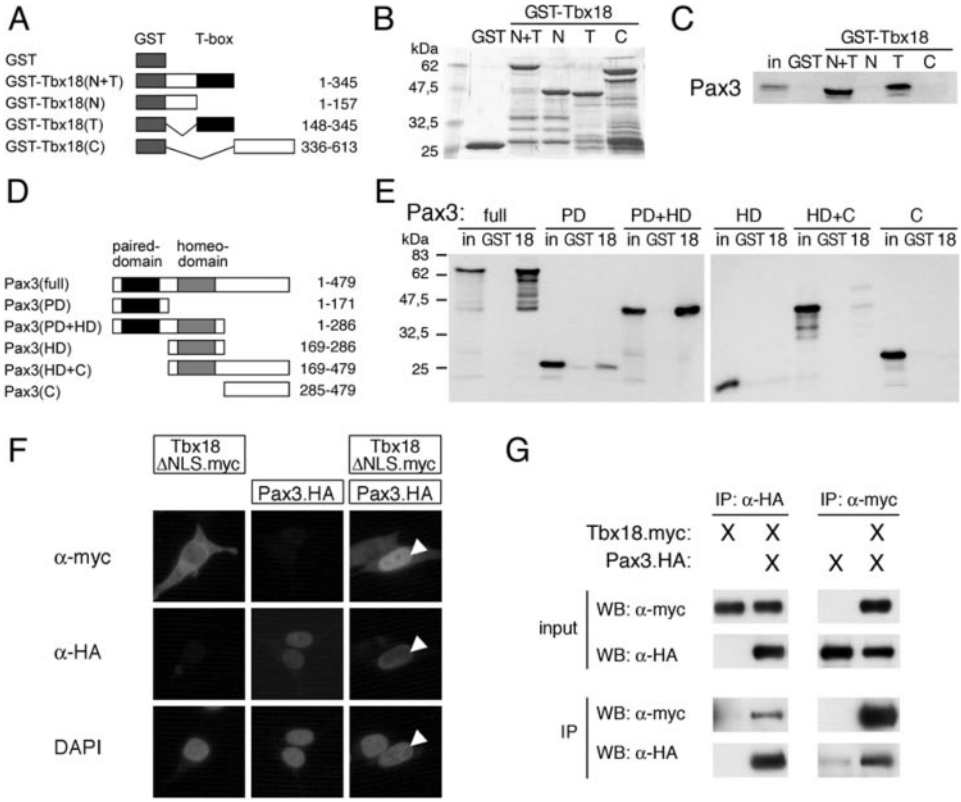

FIGURE 1. **Tbx18 and Pax3 interact *in vitro*.** *A–C*, mapping of the Tbx18 interaction domain with Pax3. *A*, schematic representation of the GST-Tbx18 deletion mutants used in this study; the T-box (*T*) is *shaded* in *black*, and N- and C-terminal domains (*N* and *C*) are shown in *white*. The *numbers* refer to the length of the expressed proteins in aa. *B*, Coomassie Brilliant Blue-stained gel of the purified GST-Tbx18 proteins. *C*, Western blot analysis of HA-tagged Pax3 protein in GST pull-downs. The T-box region of Tbx18 mediates binding to Pax3. *D*, schematic representation of a series of the Pax3 deletion mutants (HA-tagged) with the paired domain (*PD*) marked in *black* and the homeodomain (*HD*) marked in *gray*. *E*, binding analysis of Pax3 peptides to GST alone or GST-Tbx18(N+T) protein (*18*). The paired box region of Pax3 mediates binding to Tbx18. 10% of the input fraction (*in*) was loaded as control. *F*, Pax3 mediates nuclear recruitment of Tbx18ΔNLS in HEK293 cells. HEK293 cells were transfected with expression constructs for Myc-tagged NLS-deficient Tbx18 (Tbx18ΔNLS; *upper row*) in the presence or absence of HA-tagged full-length Pax3 protein (*middle row*). The *white arrowhead* indicates that Tbx18ΔNLS is efficiently relocalized to the nucleus upon co-expression of Pax3 (compare 4′,6-diamidino-2-phenylindole (*DAPI*) nuclear counter staining). *G*, complex formation between Myc-tagged Tbx18 and HA-tagged Pax3 as revealed by co-immunoprecipitation assays in transfected HEK293 cells. Western blot (*WB*) analysis of input fractions and immunoprecipitates (*IP*) using anti-HA or anti-Myc antibodies.

Pax3, additionally contain a homeodomain as a second DNA-binding region. Pax3 peptides containing the paired domain were efficiently bound to GST-Tbx18(N+T), whereas peptides containing the homeodomain only and/or the C terminus of Pax3 were not efficiently retained (Fig. 1*E*). In summary, our *in vitro* binding assays showed that binding of Tbx18 and Pax3 is mediated by the two conserved DNA binding regions, the T-domain and the paired domain.

The interaction between Tbx18 and Pax3 was additionally validated in a mammalian cell system using a nuclear recruitment assay. Transfection of an expression construct for HA-tagged Pax3 revealed constitutive nuclear localization of Pax3. In contrast, Myc-tagged Tbx18 protein lacking the nuclear localization signal (Tbx18ΔNLS) (13) was excluded from the nucleus and localized to the cytoplasm. Upon co-transfection of constructs encoding HA-tagged Pax3 protein and Myc-tagged Tbx18ΔNLS protein, nuclear localization of Tbx18 was regained (Fig. 1*F*), suggesting that Tbx18ΔNLS in complex with Pax3 is shuttled to the nuclear environment.

Furthermore, co-immunoprecipitation assays were performed in HEK293 cells transfected with full-length constructs for Myc-tagged Tbx18 alone or in the presence of HA-tagged Pax3. In immunoprecipitates obtained with the HA antibody, an enrichment of Myc-tagged Tbx18 protein was detected only upon co-transfection of the Pax3 expression construct (Fig. 1*G*, *left*). Conversely, Pax3.HA protein was specifically coimmunoprecipitated with the anti-Myc antibody when Tbx18.Myc protein was present (Fig. 1*G*, *right*), providing further proof for complex formation of Tbx18 and Pax3 in a cellular system.

T-box and Paired Box Interaction Is Promiscuous—We next investigated whether binding of Tbx18 to Pax3 is unique among T-box and Pax proteins or whether Tbx18 and Pax3 interact with additional members of the other family as well. In a GST pull-down assay, we found that, similar to Pax3, the closely related Pax7 and the more divergent proteins Pax1 and Pax9 exhibited binding to the T-domain of Tbx18 (Fig. 2*A*). This interaction was confirmed in the nuclear recruitment assay, where Tbx18ΔNLS was shuttled to the nucleus upon co-expression of HA-tagged Pax1 and Pax9 but not with unrelated nuclear proteins (data not shown).

Conversely, we analyzed if Pax3 is able to bind to other members of the T-box protein family. Therefore, GST fusions of the T-box region of the closely related Tbx15, Tbx18, and Tbx22 proteins and the distant family member Brachyury (Fig. 2*B*) were expressed in bacteria, purified (Fig. 2*C*), and incubated with *in vitro* expressed Pax3 protein. Binding of Pax3 protein was detected to all T-box proteins analyzed; however, binding of Pax3 to Tbx18 was the strongest (Fig. 2*D*).

Together, these findings suggest promiscuity of binding between T-box and paired box regions, but binding affinities between individual family members might differ substantially.

Comparative Expression Analysis of Tbx15, Tbx18, Tbx22, and Pax3—The facts that we only detected Pax3 but not other Pax family member in our yeast two-hybrid screen and the high affinity binding of Tbx18 with Pax3 in the *in vitro* assays prompted us to analyze whether this interaction is functionally relevant *in vivo*. To determine in which tissues such a molecular interaction may occur, we compared the expression patterns of *Pax3* and *Tbx18* and the two closely related *Tbx15* and *Tbx22* genes using *in situ* hybridization analysis of E9.5 wild-type mouse embryos (Fig. 3).

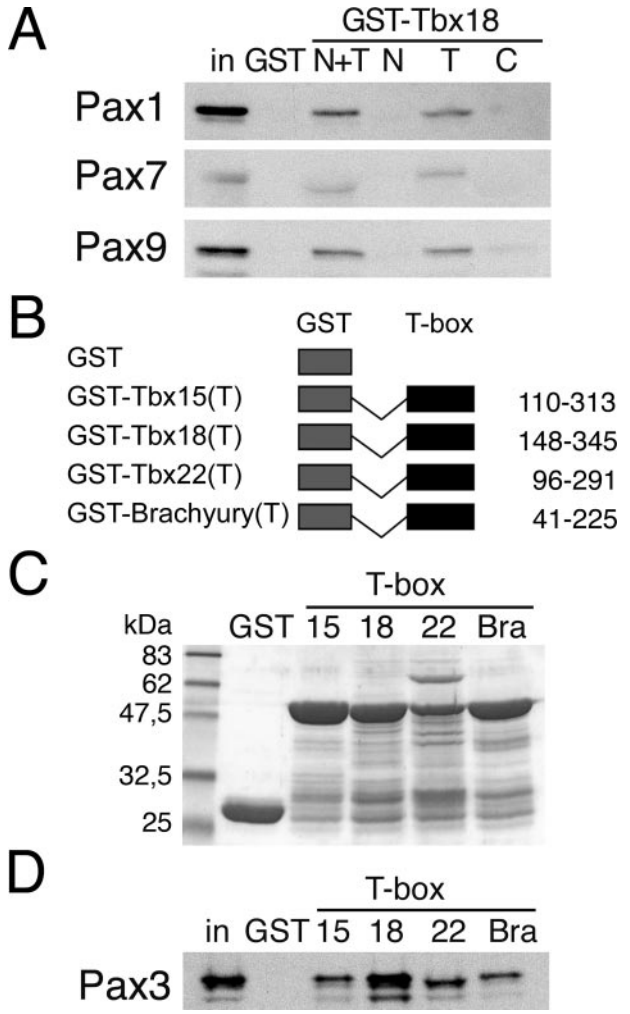

FIGURE 2. **Interaction between T-box and paired box regions is promiscuous.** *A*, Western blot analysis of HA-tagged full-length Pax1, Pax7, and Pax9 proteins in GST pull-downs with GST-Tbx18 fusion protein, as shown in Fig. 1. *B*, schematic representation of GST fusion proteins of the T-box regions of Tbx15, Tbx18, Tbx22, and Brachyury (*Bra*). *C*, visualization of purified GST proteins by Coomassie Brilliant Blue staining. *D*, Western blot analysis of HA-tagged Pax3 protein in GST pull-downs.

At this stage, *Tbx15* expression was confined to the mesenchyme of the forelimb buds (Fig. 3*A*, *arrow*). *Tbx18* was co-expressed with *Tbx15* in this tissue (Fig. 3*B*, *arrow*) but showed additional expression domains in the sinus venosus, the proepicardial organ (Fig. 3*B*, *white arrowhead*), and the head mesenchyme (Fig. 3*B*, *black arrowhead*). In derivatives of the paraxial mesenchyme, *Tbx18* expression was observed in the anterior halves of epithelial somites and additionally in two stripes representing the anterior halves of somites that were about to form (*S0* and *S−1*) (Fig. 3*E*). With differentiation of somites, *Tbx18* expression in anterior somite halves became restricted to the lateral sclerotome (Fig. 3*E*, arrow). *Tbx15* expression was absent during somite development (Fig. 3*A*). However, the closely related *Tbx22* gene was co-expressed with *Tbx18* in anterior halves of somitomeres and early somites (*S−1* to *S1*) (Fig. 3, *C* and *F*). Expression of *Tbx22* in anterior somite halves was then rapidly down-regulated, but expression was reinitiated in forming myotomes (Fig. 3*F*, *arrow*).

Pax3 was strongly expressed in the dorsal neural tube (Fig. 3*D*, *arrow*). Furthermore, *Pax3* expression was found in the anterior PSM and in epithelial somites (Fig. 3, *D* and *G*). Expression was maintained in the dermomyotomal compartment (Fig. 3*G*, *arrow*) and in migrating precursors of the limb musculature (Fig. 3*D*, *arrowhead*) (17).

Hence, *Tbx18*, *Tbx22*, and *Pax3* are co-expressed in the PSM and undifferentiated somites, but expression domains segregate during the differentiation of the sclerotome, myotome, and dermomyotome.

Tbx18 and Pax3 Cooperate in the Development of the Axial Skeleton—The observed physical interaction and the co-expression of *Tbx18* (and *Tbx22*) with *Pax3* during somitogenesis suggested that these factors also interact genetically during this process. We analyzed this possibility by generating embryos compound mutant for null alleles of *Tbx18* ($Tbx18^{GFP}$) and *Pax3* ($Pax3^{lacZ}$). On the outbred background on which we maintained these alleles, $Pax3^{-/-}$ embryos were viable at E14.5. This is in contrast to studies where lethality of $Pax3^{-/-}$ embryos was observed between E13.5 and E14.5 when the mutant allele was kept on an inbred background, such as a mix of C3H/101 and BA/Ca or C57Bl6 (17, 18). $Tbx18^{-/-}$ embryos died shortly after birth as reported before (12).

Mice double heterozygous for $Tbx18^{GFP}$ and $Pax3^{lacZ}$ mutant alleles were viable and fertile and were intercrossed to obtain all possible allelic combinations. We harvested embryos at E14.5 and analyzed the skeletons as a read-out of defects of somite patterning and differentiation. We noted that embryos double homozygous for *Pax3* and *Tbx18* null alleles were severely underrepresented at this stage. Of a total of 123 embryos harvested, we only obtained two double mutants (1.6%) instead of the expected eight (1 of 16; 6.3%). Similarly, the observed number of nine $Tbx18^{-/-}$,$Pax3^{+/-}$ embryos (7.3%) displayed a reduction from the expected value (15 embryos; 1 of 8; 12.5%), suggesting that the removal of one or two copies of one wild-type allele in the mutant background of the other gene dramatically enhanced the severity of the embryonic defects. All other genotypes were found in the expected Mendelian frequencies (data not shown).

In wild-type embryos of E14.5, the cartilagenous preskeleton was invested with a segmental array of orderly spaced ribs and vertebra (Fig. 4*A*). At the thoracic level, ribs were connected to vertebral pedicles (Fig. 4*G*, *black arrowhead*).

Strikingly, in 12 of 30 embryos (40%) double heterozygous for both *Tbx18* and *Pax3* null alleles, we detected isolated expansions of proximal ribs (Fig. 4, *B* and *H*, *white arrowhead*), whereas these malformations were never observed in single heterozygous embryos.

In $Tbx18^{-/-}$ embryos, pedicles and proximal ribs were expanded and formed contiguous cartilagenous bands in the vertebral column at the cervical and thoracic levels and the rib cage, respectively (Fig. 4, *C* (*brackets*) and *I* (*arrowheads*)) (12).

In all $Tbx18^{-/-}$,$Pax3^{+/-}$ embryos analyzed ($n = 9$), expansions of proximal ribs were increased in frequency and extended more caudally (Fig. 4*D*, *brackets*) and medially (Fig. 4*J*, *white arrowheads*) compared with $Tbx18^{-/-}$ embryos. A further expansion of pedicles was not observed (Fig. 4*J*, *black arrowhead*).

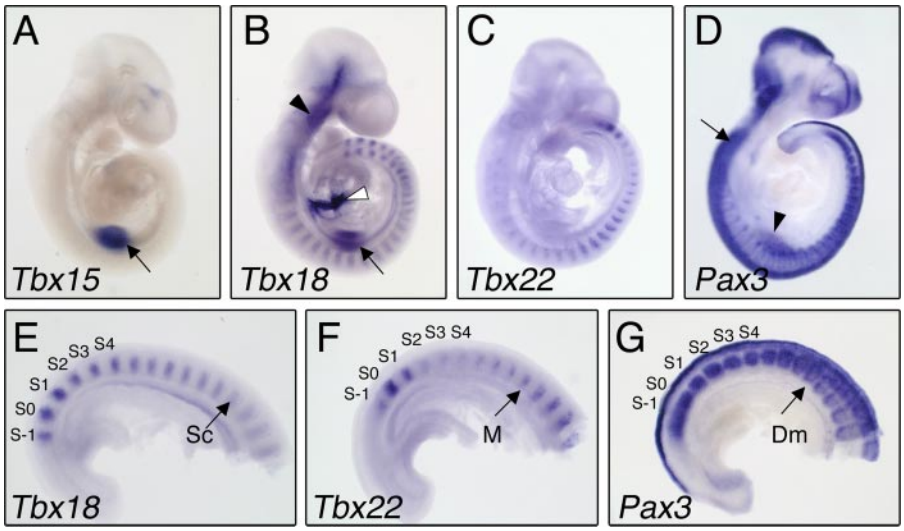

FIGURE 3. **Comparative expression analysis of *Tbx15*, *Tbx18*, *Tbx22*, and *Pax3*.** Whole mount *in situ* hybridization analysis of E9.5 wild-type mouse embryos using RNA probes specific for *Tbx15* (*A*), *Tbx18* (*B* and *E*), *Tbx22* (*C* and *F*), and *Pax3* (*D* and *G*). *A–C*, overview of the expression of *Tbx15* (*A*) in forelimb buds (*arrow*); *Tbx18* (*B*) in the mesenchyme of the forelimb (*arrow*), the proepicardial organ and sinus venosus (*white arrowhead*), and head mesenchyme (*black arrowhead*); and *Tbx22* (*C*). *D*, expression of *Pax3* in the dorsal neural tube (*arrow*) and precursors of limb muscles (*arrowhead*). *E–G*, higher magnification of expression domains in somitogenesis; presumptive (*S−1* and *S0*) and newly formed somites (*S1–S4*) are labeled. *E*, *Tbx18* is expressed in anterior halves of somitomeres (*S0* and *S−1*), epithelial somites, and differentiating sclerotomes (*Sc*). *F*, *Tbx22* in somitomeres and early somites (*S−1* to *S1*) and in the forming myotomes (*M*). *G*, *Pax3* expression can be seen in the anterior PSM (*S−1* to *S0*), the entire epithelial somite, and later in the dermomyotome (*Dm*).

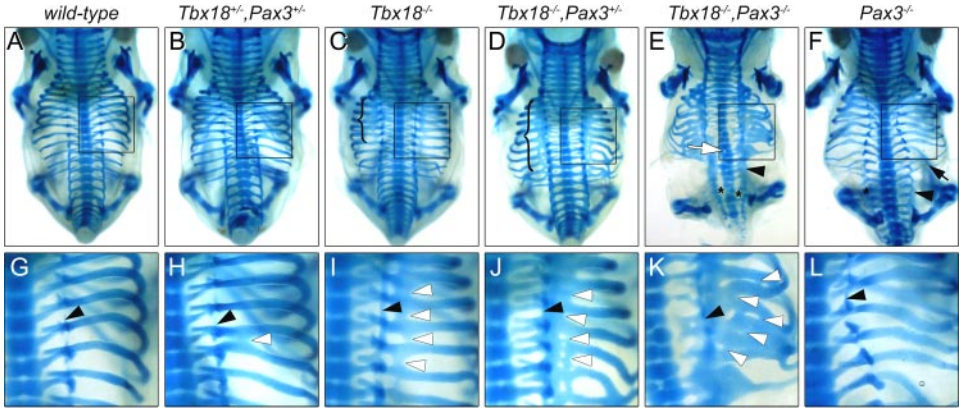

FIGURE 4. **Dose-dependent requirement of *Tbx18* and *Pax3* in the formation of the axial skeleton.** Alcian blue-stained preparations of cartilaginous preskeletons of E14.5 *Tbx18/Pax3* compound mutant embryos with genotypes indicated on the *top*. *A–F*, dorsal views; *G–L*, magnifications of the *boxed regions*. The arrangement of pedicles (*black arrowheads*) and proximal ribs (*white arrowheads*) is highlighted. In contrast to wild-type embryos (*A* and *G*), a fraction of $Tbx18^{+/-}$,$Pax3^{+/-}$-embryos (12 of 30; 40%) displays expansions of proximal ribs (*B* and *H*). $Tbx18^{-/-}$ embryos show contiguous bands of proximal ribs (*C*, *bracket*) and expanded pedicles (*I*, *black arrowhead*). Rib defects are further increased in severity in $Tbx18^{-/-}$,$Pax3^{+/-}$ compound (*D*, *bracket*; *J*, *white arrowheads*) and $Tbx18^{-/-}$,$Pax3^{-/-}$ double homozygous embryos (*K*, *white arrowheads*). In $Tbx18^{-/-}$,$Pax3^{-/-}$ embryos, pedicles and neural arches are contiguous in thoracic and lumbar regions (*E* and *K*, *black arrowheads*) and frequently unconnected to the vertebral bodies (*E*, *asterisks*). The *white arrow* indicates split vertebra. In contrast, fusions of neural arches in *Pax3* single mutants are present mainly in lumbar regions (*F*, *arrowhead*), and rib fusions and bifurcations occur more distally (*F*, *arrow*).

In mutants double homozygous for *Tbx18* and *Pax3* null alleles, the body axis was dramatically shortened ($n = 2$; Fig. 4*E*). The severity of the skeletal defects in cervical vertebrae was unchanged compared with *Tbx18* mutant embryos. In contrast, the lateral parts of the vertebrae, neural arches and pedicles, were largely expanded at the thoracic and lumbar level (Fig. 4*E*, *black arrowhead*) and frequently misconnected to the vertebral bodies that were often split (Fig. 4*E*, *asterisks* and *white arrow*, respectively). Proximal parts of ribs constituted large contiguous plates of cartilage on both sides of the vertebral column (Fig. 4*K*, *white arrowheads*).

In $Pax3^{-/-}$ embryos, defects of the axial skeleton, including fusions of neural arches of adjacent vertebrae, occurred mainly in the lumbosacral region (Fig. 4*F*, *arrowhead*), and rib fusions and bifurcations were apparent (Fig. 4*F*, *arrow*). However, skeletal defects were generally less severe than the ones described for *Pax3* alleles maintained on inbred genetic backgrounds (17, 18). Notably, and in contrast to *Tbx18* mutants, the proximal ribs were unaffected, and the pedicles were spaced regularly (Fig. 4*L*).

Together, our results demonstrate genetic interaction of *Pax3* and *Tbx18* in the formation of the axial skeleton. Removal of *Pax3* function enhances the phenotypic changes associated with the loss of *Tbx18*, namely the expansion of derivatives of the posterior lateral sclerotome, pedicles, and proximal ribs.

Tbx18 and Pax3 Cooperate in the Maintenance of Anterior Somite Halves—Co-expression of *Tbx18* and *Pax3* in undifferentiated somites suggests that not only the lateral sclerotome but also other somitic compartments could be affected by the combined loss of *Pax3* and *Tbx18* functions. To determine patterning and differentiation of the somitic mesoderm into myotome and sclerotome more carefully, we analyzed expression of molecular markers at E10.5. Within the collected embryos at this stage ($n = 221$), all genotypes were found in the expected frequencies, indicating that lethality of *Tbx18/Pax3* double mutant embryos occurred between E10.5 and E14.5.

In the E10.5 wild-type embryo, *Myogenin* was expressed in the myotomes in a repeating metameric pattern (Fig. 5*A*) (19). In $Pax3^{-/-}$ embryos, *Myogenin* was segmentally expressed in myotomes, but its hypaxial domain appeared truncated (Fig. 5*C*, *arrowhead*). This is in agreement with the known role of Pax3 as a regulator of migration and survival of myotomal cells (20–23). In *Tbx18* mutant embryos, *Myogenin* expression was unchanged (Fig. 5*B*), and no increase of the $Pax3^{-/-}$ phenotype was observed in double mutants

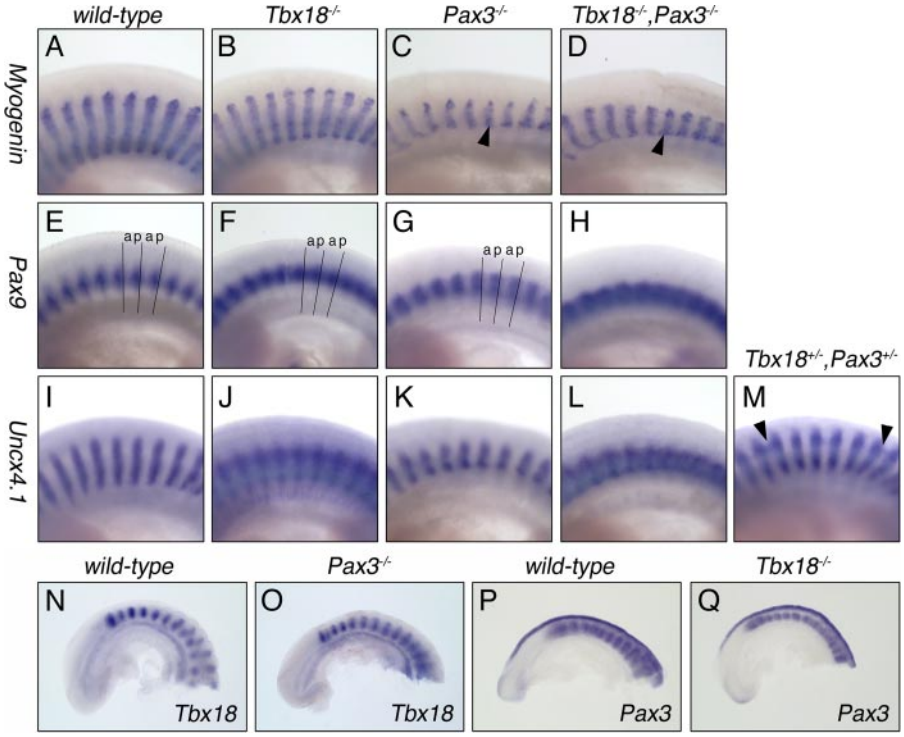

FIGURE 5. ***Tbx18* and *Pax3* cooperate in AP-somite compartmentalization.** *A–M*, expression analysis of somite differentiation markers in E10.5 *Tbx18/Pax3* compound mutant embryos. Lateral views of differentiated somites at the interlimb level, with anterior to the *left*. Genotypes are indicated on *top*. *A–D*, *Myogenin* expression reveals that combined loss of *Tbx18* and *Pax3* does not affect formation of the myotome. The hypaxial domain of the dermomyotome is truncated equally in $Pax3^{-/-}$ (*C*) and $Tbx18^{-/-}$,$Pax3^{-/-}$ embryos (*D*, *arrows*). *E–H*, polarized expression of the lateral sclerotome marker *Pax9* is cooperatively regulated by *Tbx18* and *Pax3*. Segment boundaries are highlighted with *black lines*, demonstrating expansion of *Pax9* expression in $Tbx18^{-/-}$ embryos into anterior (*a*) somite halves (*F*). In $Tbx18^{-/-}$ $Pax3^{-/-}$ embryos ($n = 3$), *Pax9* expression appears almost homogenous between anterior and posterior (*p*) somite halves (*H*). Note that in somites of $Pax3^{-/-}$ embryos, polarization of *Pax9* expression is normal (*G*). *I–M*, restriction of *Uncx4.1* expression to the sclerotome of posterior somite halves depends on both *Tbx18* and *Pax3*. Anterior expansion of *Uncx4.1* somite expression in $Tbx18^{-/-}$ embryos (*J*) is further increased by additional loss of *Pax3* ($n = 2$) (*L*). Note that in $Pax3^{-/-}$ embryos, *Uncx4.1* is restricted to the sclerotome of posterior somite halves ($n = 2$) (*K*). Isolated expansions of adjacent *Uncx4.1*-positive segments were observed in 3 of 10 $Tbx18^{+/-}$,$Pax3^{+/-}$ embryos (*M*, *arrowheads*). *N–Q*, comparative *in situ* hybridization analysis of *Tbx18* expression in E9.5 wild-type (*N*) and $Pax3^{-/-}$ embryos (*O*) and of *Pax3* expression in E9.5 wild-type (*P*) and $Tbx18^{-/-}$ embryos (*Q*) shows that somitic expression of *Tbx18* and *Pax3* is independent of each other.

(Fig. 5*D*, *arrowhead*), indicating that both genes do not cooperate in the myogenic program.

Next we analyzed *Pax9* that is expressed in the ventro-lateral sclerotome compartment with a strong up-regulation in the posterior somite halves in wild-type embryos (Fig. 5*E*) (24). In $Pax3^{-/-}$ embryos, polarized expression of *Pax9* was maintained, whereas in $Tbx18^{-/-}$ mutant embryos, *Pax9* expression became progressively homogenous with somite maturation (Fig. 5*F*). In $Tbx18^{-/-}$,$Pax3^{-/-}$ embryos ($n = 3$), *Pax9* expression was homogeneously strong in somites along the entire axial extension (Fig. 5*H*), suggesting that *Pax3* cooperates with *Tbx18* in AP-somite polarization.

To further analyze AP-somite patterning in *Tbx18/Pax3* compound mutant embryos, we used *Uncx4.1* as a marker of the posterior somite half and the caudo-lateral sclerotome (Fig. 5*I*) (9). In *Tbx18* mutant embryos, *Uncx4.1* expression was progressively expanded, demonstrating the gain of posterior and the loss of anterior somite fates (Fig. 5*J*) (12). In *Pax3* mutant embryos ($n = 2$), the domain of *Uncx4.1* was reduced in its dorso-ventral extension. However, AP polarization of expression was largely unaffected (Fig. 5*K*). In $Pax3^{-/-}$,$Tbx18^{-/-}$ embryos ($n = 2$), up-regulation of *Uncx4.1* expression was even enhanced compared with $Tbx18^{-/-}$ embryos, demonstrating a further expansion of posterior somitic identity (Fig. 5*L*). In embryos heterozygous mutant for *Pax3* or *Tbx18*, *Uncx4.1* expression was normal. In contrast, in 3 of 10 double heterozygous embryos, expansions of *Uncx4.1* expression into anterior halves of differentiated somites were detected (Fig. 5*M*, *arrowheads*).

Cooperativity of *Pax3* and *Tbx18* in AP polarization of somites may also derive from mutual regulation of the two genes in early somitogenesis. However, unchanged expression of *Tbx18* in $Pax3^{-/-}$ somites (Fig. 5*O*) and of *Pax3* in $Tbx18^{-/-}$ embryos (Fig. 5*Q*) indicates that genetic cooperativity more likely stems from co-regulation of transcriptional target genes.

Genetic Interactions in the Development of the Scapula Blade—Upon inspection of the skeletal preparations of E14.5 *Tbx18/Pax3* compound mutant embryos (for numbers see above), we detected additional defects in the appendicular skeleton indicative of a genetic interaction of the two genes in scapula development. In 4 of 19 embryos of the $Tbx18^{+/-}$,$Pax3^{-/-}$ genotype (21%), a central hole was present in the scapular blades on both sides (Fig. 6*E*). This phenotype was not observed in $Tbx18^{-/-}$ and $Pax3^{-/-}$ single or in $Tbx18^{-/-}$,$Pax3^{+/-}$ compound mutant embryos (Fig. 6, *A–D*), demonstrating a stronger contribution of *Pax3* in the genesis of this phenotypic trait. Interestingly, the appendicular skeleton of the pelvic girdle was unaffected (data not shown).

Since a similar scapula phenotype has been reported for mice homozygous mutant for *Tbx15* (15, 25), the gene most closely related to *Tbx18*, we decided to test whether *Pax3* shows genetic interaction with *Tbx15* in scapula development as well. All combinations of compound mutants were found in the expected ratio in E14.5 embryos ($n = 63$).

Similar to *Tbx18*, we observed the scapula defect in $Tbx15^{+/-}$,$Pax3^{-/-}$ embryos (Fig. 5*F*), although with a much higher penetrance (5 of 7 embryos; 71%). In addition, we noted that loss of *Pax3* in the *Tbx15* mutant background caused a dose-dependent increase in the phenotypic severity of the scapula defects (Fig. 5, *G–I*). In fact, in *Tbx15*,*Pax3* double mutant embryos, the proximal region of the scapula was almost completely absent (Fig. 5*I*).

Comparative expression analysis of *Pax3* and *Tbx15*, *Tbx18*, and *Tbx22* during limb development revealed co-expression of *Tbx15* and *Tbx18* in mesenchymal precursor cells of the scap-

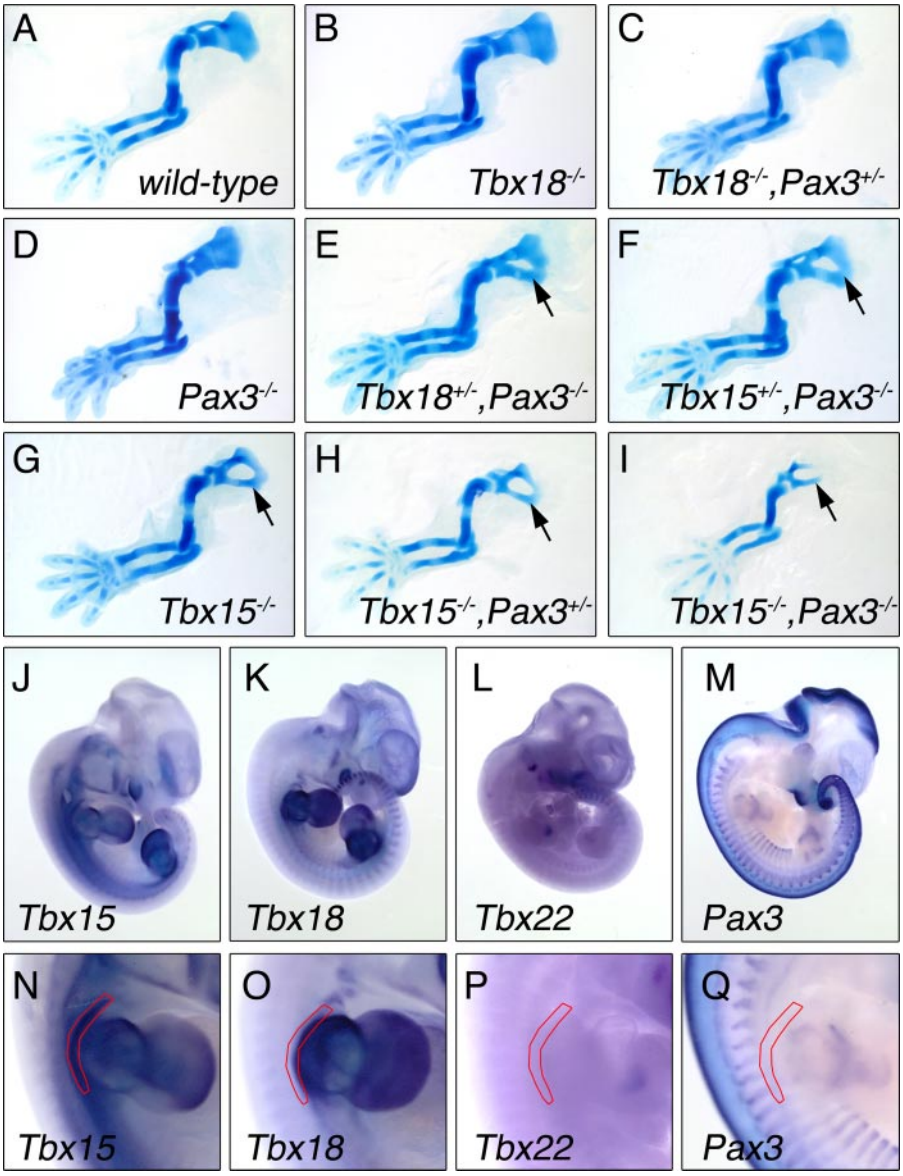

FIGURE 6. **Genetic interaction between *Pax3* and *Tbx18*/*Tbx15* in the development of the scapula blade.** *A–I*, Alcian blue-stained preparations of cartilaginous preskeletons of E14.5 forelimbs of compound mutant embryos. Limbs of $Tbx18^{-/-}$ (*B*) and $Pax3^{-/-}$ (*D*) single mutants were unaffected. However, in 4 of 19 $Tbx18^{+/-}$,$Pax3^{-/-}$ embryos (21%), a central hole in the scapula blade is present (*E*, *arrow*). In an allelic series of *Pax3* and *Tbx15* mutant alleles, we noted a similar defect in $Tbx15^{+/-}$,$Pax3^{-/-}$ embryos (*F*) although with an increased frequency (5 of 7 embryos; 71%). The scapula defect of $Tbx15^{-/-}$ (*G*) embryos increases in severity with the additional loss of one (*H*) or both alleles (*I*) of *Pax3* (*arrows*). *J–Q*, comparative expression analysis of *Tbx15* (*J* and *N*), *Tbx18* (*K* and *O*), *Tbx22* (*L* and *P*), and *Pax3* (*M* and *Q*) in the forelimb region. Shown is an overview of expression patterns in E11.5 wild-type embryos (*A–I*) and a higher magnification of forelimb buds (*N–Q*). *Tbx15* and *Tbx18* are co-expressed in the proximal region of the limb bud, whereas *Tbx22* and *Pax3* are not expressed. In *N–Q*, the scapula-forming region (26) is surrounded with a *red line*.

ula in the proximal region of the E11.5 embryo limb bud (Fig. 6, *J*, *K*, *N*, and *O*) (26). Expression of *Tbx22* was not detected in this region (Fig. 6, *L* and *P*). Surprisingly, *Pax3* was not expressed in these cells (Fig. 6, *M* and *Q*), suggesting that scapular defects might arise from an earlier requirement of *Tbx15*, *Tbx18*, and/or *Pax3* in precursor cells of the somitic mesoderm from which the scapula is derived.

DISCUSSION

Members of the T-box and the paired box families of transcriptional regulators control a diverse array of processes during vertebrate embryonic development. Here, we provide evidence that two individual members of these gene families, *Tbx18* and *Pax3*, cooperatively regulate subprograms in the development of the axial and appendicular skeletons. Direct interaction of Tbx18 and Pax3 proteins *in vitro* and in mammalian cells, co-expression of *Tbx18* and *Pax3* in the anterior PSM and in newly formed somites, and enhancement of phenotypic defects of *Tbx18* mutant embryos upon loss of *Pax3* gene function in the derivatives of the lateral sclerotome and the scapula blade suggest that these proteins cooperatively regulate gene expression programs necessary for the maintenance of the AP-somite compartmentalization and the formation of the scapula blade.

Tbx18 and Pax3 Cooperate in the Maintenance of AP-somite Polarity—Loss-of-function mutations of *Pax3* cause a wide array of developmental defects. In mice, the spontaneous *Pax3* mutation *Splotch* causes the lack of limb muscles, spina bifida and exencephaly, and defects in neural crest derivatives (27). Human patients with impaired *Pax3* function suffer from Waardenburg syndrome (28), a disease complex characterized by varying degrees of deafness, defects in structures arising from the neural crest, and pigmentation anomalies. These defects have been conceptualized by a functional requirement for *Pax3* in survival, migration, and differentiation of the hypaxial dermomyotome and the neural crest (20–23).

In the present study, we report on the genetic interaction of *Pax3* and *Tbx18* that results in phenotypic alterations affecting the development of the axial skeleton, demonstrating that beyond its well established function in the dermoyotome, *Pax3* also affects the development of the sclerotomal lineage.

In *Tbx18* mutant embryos, pedicles, and proximal ribs, derivatives of the posterior lateral sclerotome are expanded. This phenotype was traced back to a failure in maintaining the compartmentalization of somites into distinct anterior and posterior halves (12). The severity of the *Tbx18* mutant phenotype was dose-dependently increased by loss of one or two alleles of *Pax3*, resulting in an even stronger loss of anterior somite identity and expansion of elements derived from the posterior

somite halves. Most notably, in double heterozygous embryos, we observed expansions of proximal ribs, which we never detected in single heterozygotes. On the molecular level, these phenotypic changes were paralleled by a further expansion of the expression domain of *Uncx4.1*, demonstrating a requirement of both *Pax3* and *Tbx18* in maintenance of the anterior somite fate.

Tbx18 and *Pax3* are coexpressed in the anterior PSM and epithelial somites, but expression domains subsequently segregate to the anterior lateral sclerotome in the case of *Tbx18* and the dermomyotome for *Pax3*, respectively. This and the finding that Pax3 and Tbx18 interact on the protein level (see below) suggest that Pax3 and Tbx18 cooperativity results from molecular interaction occurring in early somite development.

It is noteworthy that a functional requirement for *Pax3* in early somite development has previously also been suggested by Schubert *et al.* (17), who studied defects of the axial skeleton in the *Pax3* mutant mice maintained on the C57/Bl6 inbred genetic background. There, defects in AP-somite patterning and disturbed somite boundaries were noted and also correlated with *Pax3* expression during early somite formation. The skeletal phenotype of *Tbx18*/*Pax3* double heterozygous embryos exhibited a partial penetrance only, further indicating that the function of *Pax3* is subject to genetic modification. Genetic modifiers might be represented by other members of the T-box and paired box gene families that are co-expressed with *Pax3* and *Tbx18* in early somitogenesis. We have shown that *Tbx22*, a gene closely related to *Tbx18*, is co-expressed with *Tbx18* in anterior somite halves and exhibits similar biochemical properties (13, 29). Similarly, *Pax3* gene function might be partially compensated by *Pax1* and *Pax9*, which are co-expressed with *Pax3* in early somites (24). Since we have shown that Pax3 can bind to other T-box family members, including Tbx22, and that Tbx18 can also interact with Pax1 and Pax9 *in vitro*, a complex network of Pax and T-box proteins may cooperate in early somite development.

The *Tbx18*/*Pax3* double mutants displayed contiguous cartilagenous elements, similar to *Mesp2* mutant embryos, which have completely caudalized somites (30). Moreover, isolated expansions of proximal ribs, as seen in the *Tbx18*/*Pax3* double heterozygotes, have also been reported for a hypomorphic allele of *Mesp2* (31). Although the expression of *Mesp2* is unchanged in *Tbx18*/*Pax3* double mutants (data not shown), the somitic expression of *Tbx18* is absent, and the expression of *Pax3* is strongly reduced in *Mesp2* null embryos (32, 33), arguing that after the establishment of somite AP polarity, *Tbx18* and *Pax3* act downstream of *Mesp2* to maintain AP-somite compartmentalization.

The cellular and genetic programs that are co-regulated by Tbx18 and Pax3 are currently unclear. We have previously hypothesized that Tbx18 controls maintenance of anterior somite fates by direct repression of *Delta-like 1* (*Dll1*) transcription (13) and, thus, suppression of Notch signaling that confers posterior somite fates (7). When testing the same *Dll1* promoter fragment in transactivation assays using HeLa cells, we failed to detect a cooperative effect of Pax3 and Tbx18 on *Dll1* repression (data not shown). However, elements mediating Pax3 binding may reside in promoter regions outside the fragment tested. A role for Pax3 as a transcriptional repressor that synergizes with Tbx18 is compatible with the described interaction of Pax3 with the transcriptional co-repressors HIRA and Daxx (34).

Pax3 and Tbx18 Interaction Is Mediated by Conserved DNA-binding Regions—In this study, we identified Pax3 as a binding partner of Tbx18 in a yeast two-hybrid screen and validated this interaction *in vitro* and in mammalian cells. We mapped the interaction domain to the T-box region of Tbx18 and the paired domain of Pax3, demonstrating that these DNA-binding domains have an additional role as protein-protein interaction motifs. Although we and others have shown that the T-box region mediates binding to the homeobox region in other homeodomain transcription factors, including Nkx2-5 (13, 35), the homeodomain of Pax3 was not efficiently bound by Tbx18, suggesting that interaction of DNA-binding regions is selective.

However, we found that the interaction between paired box and T-box regions is promiscuous among divergent members of both families, suggesting functional co-operativity of other T-box and Pax proteins in tissues of co-expression. One example has previously been presented by the pair of Tbx5 and Pax6 that may cooperate to regulate dorso-ventral patterning of the optic cup (36).

Interaction among different classes of DNA-binding transcription factors is likely to represent a common mechanism to increase specificity of target gene recognition. For T-box proteins, the combinatorial function with other classes of DNA-binding proteins in target promoter regulation is well established. One example is the interaction of Tbx2, Tbx5, Tbx18, and Tbx20 with the transcription factors Gata4 and Nkx2–Nkx5 to regulate cardiac expression of *Nppa* (*natriuretic peptide precursor type a*) (13, 35, 37–41). Likewise, Pax proteins have been shown to interact with a number of different DNA-binding proteins, including Pax3 interacting with Sox10 and Mox2 and Pax6 binding to pRB (34). Future approaches for the identification of target genes of Tbx18 could benefit from a search of the combined presence of conserved T-sites and paired binding sites (42).

Pax3 Cooperates with Tbx15 and Tbx18 in the Development of the Scapula Blade—Our analysis of the phenotypes of *Tbx18*/*Pax3* compound mutants uncovered an additional requirement for both genes in the formation of the scapula blade. In compound mutant embryos, the scapula blade exhibited a central hole. In addition, loss of *Pax3* dose-dependently increased the severity of the scapula defect in the mutants for *Tbx15* (15, 25), the T-box gene most highly related to *Tbx18*.

The formation of the scapula blade, the thin posterior extension of the shoulder girdle is unusual in the respect that it neither derives from the sclerotomal cells of the somite nor from the lateral plate mesoderm like the limb skeleton but from a set of eight dermomyotomes from somites 17 to 24 as revealed by chick-quail chimeric analysis (43). Hence, a common Pax3 positive pool of precursor cells contributes to both limb muscles and the scapula. Under the influence of signaling pathways from the surroundings, including the surface ectoderm, the subpool of scapula precursor cells switches expression from Pax3 to Pax1 and enters chondrogenic differentiation (44). The scapula blade is an extremely thin bone that is exquisitely sen-

sitive to slight alterations in proliferation and thus reduction of the pool of precursor cells. Since we did not detect co-expression of *Pax3* with *Tbx15* and *Tbx18* in the scapula-forming region (26), *Pax3* and *Tbx15/Tbx18* may act subsequently rather than simultaneously. Loss of *Pax3* function my lead to a reduction of the dermomyotomal precursor pool that becomes available for *Tbx15/Tbx18* to act on. Further loss of *Tbx15* and *Tbx18* function may then reduce the number of mesenchymal precursor cells of the scapula under a critical threshold required for the condensation and/or chondrification process. Alternatively, Pax3 protein may persist in the precursor cells of the scapula for some time, given an opportunity for molecular interaction with these T-box transcription factors.

Interestingly, *Tbx15* has been shown to synergize with a number of other transcription factor genes, including *Gli3* and aristaless-type homeobox genes (*Alx4* and *Cart1*) in scapula development (25), arguing for a complex network of developmental regulators involved in patterning/differentiation of this bone.

Acknowledgment—We thank Eric Olsen (Southwestern Medical Center) for the Myogenin probe.

REFERENCES

1. Goldstein, R. S., and Kalcheim, C. (1992) *Development* **116,** 441–445
2. Aoyama, H., and Asamoto, K. (2000) *Mech. Dev.* **99,** 71–82
3. Christ, B., Huang, R., and Scaal, M. (2007) *Dev. Dyn.* **236,** 2382–2396
4. Aulehla, A., and Herrmann, B. G. (2004) *Genes Dev.* **18,** 2060–2067
5. Saga, Y. (2007) *Dev. Dyn.* **236,** 1450–1455
6. Morimoto, M., Takahashi, Y., Endo, M., and Saga Y. (2005) *Nature* **435,** 354–359
7. Barrantes, I. B., Elia, A. J., Wunsch, K., Hrabe de Angelis, M. H., Mak, T. W., Rossant, J., Conlon, R. A., Gossler, A., and de la Pompa, J. L. (1999) *Curr. Biol.* **9,** 470–480
8. Kraus, F., Haenig, B., and Kispert, A. (2001) *Mech. Dev.* **100,** 83–86
9. Neidhardt, L. M., Kispert, A., and Herrmann, B. G. (1997) *Dev. Genes Evol.* **207,** 330–339
10. Leitges, M., Neidhardt, L., Haenig, B., Herrmann, B. G., and Kispert, A. (2000) *Development* **127,** 2259–2267
11. Mansouri, A., Voss, A. K., Thomas, T., Yokota, Y., and Gruss, P. (2000) *Development* **127,** 2251–2258
12. Bussen, M., Petry, M., Schuster-Gossler, K., Leitges, M., Gossler, A., and Kispert, A. (2004) *Genes Dev.* **18,** 1209–1221
13. Farin, H. F., Bussen, M., Schmidt, M. K., Singh, M. K., Schuster-Gossler, K., and Kispert, A. (2007) *J. Biol. Chem.* **282,** 25748–25759
14. Mansouri, A., Pla, P., Larue, L., and Gruss, P. (2001) *Development* **128,** 1995–2000
15. Singh, M. K., Petry, M., Haenig, B., Lescher, B., Leitges, M., and Kispert, A. (2005) *Mech. Dev.* **122,** 131–144
16. Wilkinson, D. G., and Nieto, M. A. (1993) *Methods Enzymol.* **225,** 361–373
17. Schubert, F. R., Tremblay, P., Mansouri, A., Faisst, A. M., Kammandel, B., Lumsden, A., Gruss, P., and Dietrich, S. (2001) *Dev. Dyn.* **222,** 506–521
18. Henderson, D. J., Conway, S. J., and Copp, A. J. (1999) *Dev. Biol.* **209,** 143–158
19. Edmondson, D. G., and Olson, E. N. (1989) *Genes Dev.* **3,** 628–640
20. Williams, B. A., and Ordahl, C. P. (1994) *Development* **120,** 785–796
21. Bober, E., Franz, T., Arnold, H. H., Gruss, P., and Tremblay, P. (1994) *Development* **120,** 603–612
22. Daston, G., Lamar, E., Olivier, M., and Goulding, M. (1996) *Development* **122,** 1017–1027
23. Borycki, A. G., Li, J., Jin, F., Emerson, C. P., and Epstein, J. A. (1999) *Development* **126,** 1665–1674
24. Neubüser, A., Koseki, H., and Balling, R. (1995) *Dev. Biol.* **170,** 701–716
25. Kuijper, S., Beverdam, A., Kroon, C., Brouwer, A., Candille, S., Barsh, G., and Meijlink, F. (2005) *Development* **132,** 1601–1610
26. Pellegrini, M., Pantano, S., Fumi, M. P., Lucchini, F., and Forabosco, A. (2001) *Dev. Biol.* **232,** 149–156
27. Epstein, D. J., Vogan, K. J., Trasler, D. G., and Gros, P. (1993) *Proc. Natl. Acad. Sci. U. S. A.* **90,** 532–536
28. Tassabehji, M., Read, A. P., Newton, V. E., Patton, M., Gruss, P., Harris, R., and Strachan, T. (1993) *Nat. Genet.* **3,** 26–30
29. Andreou, A. M., Pauws, E., Jones, M. C., Singh, M. K., Bussen, M., Doudney, K., Moore, G. E., Kispert, A., Brosens, J. J., and Stanier, P. (2007) *Am. J. Hum. Genet.* **81,** 700–712
30. Saga, Y., Hata, N., Koseki, H., and Taketo, M. M. (1997) *Genes Dev.* **11,** 1827–1839
31. Morimoto, M., Kiso, M., Sasaki, N., and Saga, Y. (2006) *Dev. Biol.* **300,** 687–698
32. Takahashi, Y., Yasuhiko, Y., Kitajima, S., Kanno, J., and Saga, Y. (2007) *Dev. Biol.* **304,** 593–603
33. Takahashi, Y., Takagi, A., Hiraoka, S., Koseki, H., Kanno, J., Rawls, A., and Saga, Y. (2007) *Dev. Dyn.* **236,** 1484–1494
34. Buckingham, M., and Relaix, F. (2007) *Annu. Rev. Cell Dev. Biol.* **23,** 645–673
35. Hiroi, Y., Kudoh, S., Monzen, K., Ikeda, Y., Yazaki, Y., Nagai, R., and Komuro, I. (2001) *Nat. Genet.* **28,** 276–280
36. Leconte, L., Lecoin, L., Martin, P., and Saule, S. (2004) *J. Biol. Chem.* **279,** 47272–47277
37. Bruneau, B. G., Nemer, G., Schmitt, J. P., Charron, F., Robitaille, L., Caron, S., Conner, D. A., Gessler, M., Nemer, M., Seidman, C. E., and Seidman, J. G. (2001) *Cell* **106,** 709–721
38. Garg, V., Kathiriya, I. S., Barnes, R., Schluterman, M. K., King, I. N., Butler, C. A., Rothrock, C. R., Eapen, R. S., Hirayama-Yamada, K., Joo, K., Matsuoka, R., Cohen, J. C., and Srivastava, D. (2003) *Nature* **424,** 443–447
39. Stennard, F. A., Costa, M. W., Elliott, D. A., Rankin, S., Haast, S. J., Lai, D., McDonald, L. P., Niederreither, K., Dolle, P., Bruneau, B. G., Zorn, A. M., and Harvey, R. P. (2003) *Dev. Biol.* **262,** 206–224
40. Habets, P. E., Moorman, A. F., Clout, D. E., van Roon, M. A., Lingbeek, M., van Lohuizen, M., Campione, M., and Christoffels, V. M. (2002) *Genes Dev.* **16,** 1234–1246
41. Plageman, T. F., Jr., and Yutzey, K. E. (2004) *J. Biol. Chem.* **279,** 19026–19034
42. Ovcharenko, I., and Nobrega, M. A. (2005) *Nucleic Acids Res.* **33,** W403–W407
43. Huang, R., Christ, B., and Patel, K. (2006) *Anat. Embryol.* **211,** Suppl. 1, 65–71
44. Huang, R., Zhi, Q., Patel, K., Wilting, J., and Christ, B. (2000) *Development* **127,** 3789–3794